ELSEVIER

Chemical Geology 225 (2006) 176–188

CHEMICAL GEOLOGY
INCLUDING
ISOTOPE GEOSCIENCE

www.elsevier.com/locate/chemgeo

Computer simulation of mineral solid solutions

J.A. Purton [a,*], N.L. Allan [b,1], M.Yu. Lavrentiev [c,2], I.T. Todorov [a,b], C.L. Freeman [b]

[a] CLRC, Daresbury Laboratory, Keckwick Lane, Warrington, WA4 4AD, UK
[b] School of Chemistry, University of Bristol, Cantock's Close, Bristol, BS8 1TS, UK
[c] EURATOM/UKAEA Fusion Association, Culham Science Centre, Oxfordshire, OX14 3DB, UK

Accepted 16 August 2005

Abstract

We discuss how two techniques, based on (1) lattice dynamics (lattice statics) simulations and (2) Monte Carlo methods may be used to calculate the thermodynamic properties of solid solutions and highly disordered systems. The lattice dynamics calculations involve a full free-energy structural optimisation of each of a number of configurations, followed by thermodynamic averaging. The Monte Carlo simulations include the explicit interchange of cations and use the semi-grand canonical ensemble for chemical potential differences. Both methods are readily applied to high pressures and elevated temperatures without the need for any new parameterisation. We discuss the application of the Monte Carlo technique to the study of surfaces. A range of examples, including binary oxides, spinels, carbonates and surface segregation, is used to illustrate the methods.

Keywords: Solid solutions; Monte Carlo; Lattice dynamics; Ordering; Phase diagrams; Spinels; Carbonates; Oxides

1. Introduction

The continuing growth in computer power has led to a tremendous increase in the contribution of computer simulation to the understanding of the physical and chemical properties of minerals. Atomistic simulation techniques and ab initio methods have proved extremely useful in providing detailed and accurate predictions of the structures and properties of silicate minerals. The principal objectives of these computations are to obtain insight into atomistic or microscopic processes that underlie macroscopic phenomena and to carry out simulations at pressures and temperatures beyond the accessible range of experimental techniques (see, e.g., Hazen and Downs, 2000; Purton et al., 2000). For example, calculated seismic velocity profiles can be used to supplement models of density contrasts derived from seismic tomography and test proposed compositional models for the mantle.

Geological materials are often poorly characterized since many minerals occur deep within the Earth's mantle and there are limitations in experimental techniques. This problem is acute since naturally occurring minerals contain a large number of elements, including minor and trace element impurities, which may be disordered over several crystallographic sites. Unfortunately, the present computational techniques available are largely restricted to *idealized* end-member systems (e.g., pure $MgSiO_3$ perovskite) since kinetic barriers prevent classical Monte Carlo and molecular dynamics simulations being undertaken within a realistic timescale. Contact

* Corresponding author. Tel.: +44 1925 603785.
E-mail addresses: j.a.purton@dl.ac.uk (J.A. Purton), n.l.allan@bris.ac.uk (N.L. Allan), Mikhail.Lavrentiev@ukaea.org.uk (M.Yu. Lavrentiev).
[1] Tel.: +44 117 9288308.
[2] Tel.: +44 1235 466450.

0009-2541/$ - see front matter © 2005 Elsevier B.V. All rights reserved.
doi:10.1016/j.chemgeo.2005.08.032

between experiment and theory is thus considerably restricted which is unfortunate considering the importance of solid solutions in mineral physics.

Our research has sought to address some of these problems and to describe and apply a Monte Carlo and lattice dynamics techniques that can be readily employed to study the ordering mechanisms of solid solutions and/or the thermodynamic properties of solid solutions under different conditions. A key objective of our recent work (see for example Purton et al., 1998, 1999; Allan et al., 2001a,b) is to study the phase equilibria of complex systems such as oxides, silicate melts and minerals at any given temperature and pressure. Any technique that can be applied to systems of geological interest must meet the following criteria:

1. The kinetic barriers that prevent diffusion on the time scale of atomistic simulations must be overcome by generating the large number of configurations possible within a disordered phase. This can be achieved by making random changes to the identity of the ion(s) occupying a crystallographic site and sampling a range of low energy states.
2. Ions must be allowed to "relax" fully around the impurity ion. The importance of local relaxation around defects in polar solids is much greater in oxides than in metals and has been discussed extensively in the literature (e.g., Catlow and Mackrodt, 1982).
3. Lattice vibrations should ideally be included in the calculation. However, the computational time required for some systems may prevent the inclusion of this term. The role of lattice vibrations on the stability of materials is ambiguous.
4. Methods should be extendable to different ensembles (e.g., the effects of pressure readily included in the simulation) and to surfaces.

In this brief review, we briefly discuss the atomistic simulation techniques and their application to order/disorder in spinel, the segregation of dopant ions to mineral surfaces and the calculation of the phase diagrams.

2. Method

All calculations are based on the ionic model using two-body potentials to represent the short-range forces (for a full discussion of this well-known model see, for example, Catlow and Mackrodt, 1982, and Catlow, 1997). We adopted the common Born–Mayer form for the potentials, with the O–O interaction supplemented by an r^{-6} attractive term: $V(r)=A\exp(-r/\rho)-C/r^6$, where A, C and ρ are constants. Oxide ion polarisation was accounted for via the shell model (Dick and Overhauser, 1958) during energy minimisation calculations. Of course, the success of any atomistic simulation is reliant on the accuracy of the inter-atomic potentials and in each application potentials are tested for their suitability. This is beyond the scope of this review and the reader is referred to the relevant publications below.

2.1. Monte Carlo simulations

As a starting point we describe the classical Monte Carlo technique, which is discussed in detail by Frenkel and Smit (2002), and then discuss how this has been extended for application to non-stoichiometric solids. During one step of the Monte Carlo simulation, a random decision is made to alter one of the variables of the calculation, which may either be an atomic position or the cell dimensions, i.e., all simulations are carried out within the *NPT* ensemble and lattice vibrations are automatically included (Frenkel and Smit, 2002). The magnitude of the change is also chosen at random, but within a specified amount and governed by the variables r_{max} and v_{max}, respectively. The magnitude of these variables is adjusted automatically so that the acceptance/rejection ratio is 0.3 (Allen and Tildesley, 1987). After each move/volume alteration, the change in energy is calculated and a decision whether to accept or reject this is made according to the standard Metropolis scheme (Metropolis et al., 1953). We have extended this approach to allow for the atomic configuration to evolve during the simulation (Purton et al., 1998). In addition to random movements of atoms, or cell volume we also make an exchange of two (or more) cations chosen at random again with the acceptance/rejection decision made using the Metropolis scheme. In the minerals of interest in this paper, the efficiency of this exchange is very low due to the difference in size of the cations. Low exchange rate slows the equilibration, so that special methods are necessary to increase the rate of successful exchanges. To speed up the speed of sampling configurations, we have applied the biased sampling technique, widely used in the simulation of molecules and polymers (e.g., Frenkel and Smit, 2002). In our exchange-biased Monte Carlo (Lavrentiev et al., 2001), instead of considering a single trial exchange, a set of trial exchanges is picked at random. Suppose an exchange take place between atoms A and B. First, k pairs $\{A^i, B^i, i=1,\ldots, k\}$ are randomly chosen. We denote the system energy in the initial configuration as U_{old} and the energy of the system after exchange of atoms in the ith pair (A^i,B^i) as

U^i_{new}. One of the new configurations i is then chosen with probability

$$p_i = \frac{\exp\left(-\beta\left(U^i_{\text{new}} - U_{\text{old}}\right)\right)}{W_{\text{new}}}, \beta = (kT)^{-1} \quad (1)$$

where

$$W_{\text{new}} = \sum_{i=1}^{k} \exp\left(-\beta\left(U^i_{\text{new}} - U_{\text{old}}\right)\right) \quad (2)$$

The chosen configuration i (that after the exchange of the ith pair) with energy $U_{\text{new}}{}^i \equiv U_{\text{new}}$ is then the trial configuration. However, the usual acceptance rule cannot be directly applied. Instead, starting from the new configuration, a further $k-1$ pairs A^j, B^j, $j=1,\ldots,$ $k-1$ are chosen. Denoting the energy of the system after exchange of atoms in the jth pair (A^j,B^j) U^j, we evaluate the expression

$$W_{\text{old}} = \exp(-\beta(U_{\text{old}} - U_{\text{new}})) + \sum_{j=1}^{k-1} \exp\left(-\beta\left(U^j - U_{\text{new}}\right)\right) \quad (3)$$

Fulfilling detailed balance, the criterion for the acceptance of the new configuration is

$$\text{acc}(\text{old}\rightarrow\text{new}) = \min\left[1, \exp(-\beta(U_{\text{old}} - U_{\text{new}}))\frac{W_{\text{new}}}{W_{\text{old}}}\right] \quad (4)$$

Use of the exchange-bias technique significantly improves the sampling of different configurations (Lavrentiev et al., 2001) and this rate of exchange is sufficient for convergence for the systems of interest in this paper at the temperatures we have studied. Two species were exchanged during the simulations in this review, but, the exchange-bias approach could be extended to multiple ion exchanges.

In order to calculate a phase diagram using the MC technique, it is necessary to evaluate the excess free energy, $\Delta\mu_{\text{B/A}}$, using the semi-grand canonical ensemble (Frenkel and Smit, 2002). In this method, we evaluate the potential energy change $\Delta U_{\text{B/A}}$ which would result if one species, B were to be converted into another, A. This change in energy is related to the corresponding change in chemical potential $\Delta\mu_{\text{B/A}}$ by,

$$\Delta\mu_{\text{B/A}} = -k_{\text{B}}T\ln\left\langle \frac{N_{\text{B}}}{N_{\text{A}}+1}\exp\left(-\Delta U_{\text{B/A}}/k_{\text{B}}T\right)\right\rangle. \quad (5)$$

Thus for MgO–MnO, we evaluate the energy associated with the conversion of a randomly chosen Mg ion to an Mn ion, $\Delta U_{\text{Mg/Mn}}$ and the reverse transformation. We emphasize that the change of Mg into Mn, and vice versa, is only a temporary substitution to determine the difference in chemical potential. After Eq. (5) is evaluated, the identity of the randomly chosen ion reverts to Mg (Mn) and the simulation continued as before. The semi-grand canonical ensemble is used in preference to the grand canonical ensemble since good statistics for $\Delta\mu_{\text{B/A}}$ can readily be achieved.

The simulations described above are suitable for bulk materials, in which the stoichiometry does not change. However, the surface of a crystal always provides a different elastic and electrostatic environment to that of the bulk, and so there is a free energy difference associated with all defects, including impurities, which drives them to or from the surface. Therefore, in order to simulate the surface or grain boundary of a mineral a specialised unit cell and an additional Monte Carlo step are required in the simulation. Within the simulation cell, the surfaces are assumed to be planar, semi-infinite and periodic in two dimensions (i.e., periodic boundary conditions are removed in one dimension). The simulation cell is divided into two regions; region I and region II (Mackrodt and Stewart, 1977; Tasker, 1979). The ions in region I are allowed to "relax" explicitly whereas those in region II are held fixed. All calculations are based on an ionic model using two-body potentials to represent short-range interactions (Catlow and Mackrodt, 1982). The additional Monte Carlo step forms the basis of the "transmutational" ensemble and is a specialised version of the grand canonical ensemble. In the transmutation step a cation, or anion, is chosen at random and its chemical identity is changed (i.e., A is transformed to B ion or B transformed to A). Although the ratio of A and B atoms is allowed to vary in this ensemble the total number of particles are kept constant. The change in chemical identity is accepted according to the relative probability

$$\frac{P_{\text{new}}}{P_{\text{old}}} = \mathrm{e}^{-\beta\Delta\mu}, \quad (6)$$

where $\Delta\mu$ is the chemical potential difference (Rittner et al., 1994). The value of $\Delta\mu$ is determined from a series of bulk calculations, in which $\Delta\mu$ is varied systematically until the desired concentration of ions is achieved. This ensures that, at constant number of particles, segregation at the surface is possible while the average stoichiometry in the bulk remains constant.

2.2. Lattice statics and dynamics

In the static limit, the crystal structure is determined by the condition $\partial E/\partial X_i = 0$, where E is the static contribution to the internal energy, and the variables $\{X_i\}$ define the structure (i.e., the lattice vectors, the atomic positions in the garnet unit cell, and the oxygen shell positions) (for more details, see Catlow and Mackrodt, 1982).

An alternative method for the calculation of thermodynamic properties of a *periodic* solid at finite temperature and high pressure is via the direct minimisation of the free energy (rather than just the static energy) with respect to the variables $\{X_i\}$ which define the structure.

We use quasiharmonic lattice dynamics (QLD) for the vibrational terms, in which it is assumed that the Helmholtz energy, F, of a crystal, at temperature T can be written as the sum of static and vibrational contributions (Maradudin et al., 1971),

$$F(X_i, T) = E(X_i) + F_{\mathrm{vib}}(X_i, T) \tag{7}$$

where, as before, E is the static energy. The traditional static-limit lattice simulations referred to above evaluate only E. In this static limit, F_{vib}, which is the sum of harmonic vibrational contributions from all the normal modes, is neglected.

For a periodic solid, the frequencies $\nu_j(\mathbf{q})$ of modes with wavevector $\mathbf{q}$ are obtained by diagonalisation of the dynamical matrix $D(\mathbf{q})$ (e.g., Wallace, 1972). F_{vib} is given by

$$F_{\mathrm{vib}} = \sum_{\mathbf{q},j} \left\{ \frac{1}{2} h\nu_j(\mathbf{q}) + k_{\mathrm{B}} T \ln\left[1 - \exp\left(-h\nu_j(\mathbf{q})/k_{\mathrm{B}}T\right)\right] \right\}, \tag{8}$$

where h is Planck's constant and k_{B} Boltzmann's constant. The first term on the right-hand side of Eq. (8) is the zero–point energy. The sum over the wavevectors $\mathbf{q}$ is evaluated by taking successively finer uniform grids (Chadi and Cohen, 1973) in the Brillouin zone until convergence is achieved.

At given temperature, the free energy obtained from Eqs. (7) and (8) is a function of the variables that define the structure. The equilibrium structure at any applied pressure is then that which minimises the Gibbs energy $F+PV$ with respect to all these variables. Our free energy minimisation (structure optimisation) code SHELL (Taylor et al., 1998) uses the full set of analytic derivatives of F (Taylor et al., 1997) in order to perform the minimisation efficiently.

Given the optimised structure at specified P and T and the corresponding values of F, it is straightforward to calculate other thermodynamic properties by suitable algebraic manipulation. The (vibrational) entropy S and the heat capacity C_{v} are given by

$$S = \sum_{\mathbf{q},j} \left\{ \frac{\left(h\nu_j(\mathbf{q})/T\right)}{\exp\left(h\nu_j(\mathbf{q})/k_{\mathrm{B}}T\right) - 1} - k_{\mathrm{B}} \ln\left[1 - \exp\left(-h\nu_j(\mathbf{q})/k_{\mathrm{B}}T\right)\right] \right\} \tag{9}$$

$$C_{\mathrm{v}} = \sum_{\mathbf{q},j} k \left(\frac{h\nu_j}{2kT}\right)^2 \mathrm{cosech}^2\left(\frac{h\nu_j}{2kT}\right) = k\left(\frac{h\nu_j}{kT}\right)^2 \Big/ \left[\left\{\exp\left(h\nu_j/kT\right) - 1\right\} \times \left\{1 - \exp\left(-h\nu_j/kT\right)\right\}\right] \tag{10}$$

Vibrational (phonon) densities of states may be obtained by evaluating the frequencies over a suitable grid of points over the Brillouin zone.

The quasiharmonic approximation and thus this technique breaks down with increasing amplitude of vibration and hence at high temperatures. This often occurs at $\approx 2/3$ of the melting point (Barrera et al., 1997). For any given temperature, higher pressures correspond to smaller internuclear separations and amplitudes of vibration so the breakdown of the quasiharmonic approximation can be less important for applications involving high pressure.

Below the melting point, the only states of practical importance lie at the bottom of K local minima in the energy of the system (i.e., they correspond to a given configuration) and we describe, for lattice dynamics, the statistical sampling of these configurations required for the calculation of the thermodynamic properties of solid solutions. For each configuration k, we suppose there are a number of states, which correspond to small or moderate changes in the internal and external lattice strains. States corresponding to large changes in these strains have high energies and do not contribute significantly to the equilibrium properties of the system. These are ignored. Using the label $k = 1 \ldots K$ for the configuration, then the enthalpy and Gibbs energy in the isobaric-isothermal (NPT) ensemble are given by

$$H = \frac{\sum_{k=1}^{K} H_k \exp\left(-G_k/k_{\mathrm{B}}T\right)}{\sum_{k=1}^{K} \exp\left(-G_k/k_{\mathrm{B}}T\right)} \tag{11}$$

$$G = -k_{\mathrm{B}}T \ln \sum_{k=1}^{K} \exp\left(-G_k/k_{\mathrm{B}}T\right) \tag{12}$$

G_k is the Gibbs energy for the relaxed structure of each possible cation arrangement (Allan et al., 2001a,b). We thus have expressions for any thermodynamic quantity in terms of thermodynamic quantities obtained with particular configurations. The thermodynamic averaging is performed over the results of a set of full free-energy minimisations of different arrangements (configurations) of the cations within a supercell.

It is useful to rewrite G as

$$G = -k_B T \ln K - k_B T \ln\left(\sum_{k=1}^{K} \exp(-G_k/k_B T)/K\right) \quad (13)$$

where K is the total number of possible configurations for the supercell considered. The first term in Eq. (13) is the ideal term, and the second the deviation from ideality. For other than the smallest supercells, it is impractical to sum over all K configurations and all summations in Eqs. (11) and (12) are restricted to K' configurations chosen at random; K in the second term of Eq. (13) is replaced by K'. Thus

$$H = \frac{\sum_{k=1}^{K'} H_k \exp(-G_k/k_B T)}{\sum_{k=1}^{K'} \exp(-G_k/k_B T)}, \quad (14)$$

and

$$G = -k_B T \ln K - k_B T \ln\left(\sum_{k=1}^{K'} \exp(-G_k/k_B T)/K'\right) \quad (15)$$

We show later that convergence in both these quantities can be reached using a manageable value of K'. The entropy is readily obtained from $(H-G)/T$.

The volume is given by an equation analogous to Eq. (14);

$$V = \frac{\sum_{k=1}^{K'} V_k \exp(-G_k/k_B T)}{\sum_{k=1}^{K'} \exp(-G_k/k_B T)}, \quad (16)$$

where V_k is the volume of configuration k.

Eqs. (14)–(16) involve the full free energy minimisation of each configuration at each P and T of interest. It is computationally much cheaper to optimise every configuration in the static limit. When we refer below to thermodynamic properties of the solid solutions in the static limit, configurationally averaged values are evaluated using Eqs. (14)–(16) replacing G_k with E_k. The vibrational contribution to E_k and the vibrational entropy are ignored. Not only is the minimisation of each configuration computationally cheaper, but in addition, only *one* set of runs for a given composition is required for *all* temperatures.

3. Results and discussion

We illustrate the application of the MC and QLD by way of four geologically important examples: namely the degree of order/disorder in spinels, surface segregation at MgO{001} surfaces and the thermodynamic properties of MgO–MnO and $(Ca,Mg)CO_3$ solid solutions.

3.1. Ordering in spinels

Spinels, and especially $MgAl_2O_4$, are a geologically important group of minerals. For example, $MgAl_2O_4$ may exist up to 50–80 km within the upper mantle and reacts with pyroxene to form olivine and garnet. An understanding of the thermodynamics of ordering of $MgAl_2O_4$ and thus its stability has implications for trace element partitioning of transition metals and Al with other mantle phases. Usually, the distribution of cations between tetrahedral and octahedral sites is described by the so-called inversion parameter, x: $(A_{1-x}B_x)_T(B_{2-x}A_x)_O O_4$, where subscripts T and O refer to the cations on tetrahedral and octahedral sites, respectively (Navrotsky and Kleppa, 1967; Navrotsky, 1994). However, we use an alternative description of spinels in terms of the order parameter, Q (Carpenter and Salje, 1994; Harrison and Putnis, 1999), which is defined as $Q = 1 - 3x/2$. Q varies from a value of 1 for completely normal spinels to -0.5 for completely inverse spinels. Q equals zero for a random arrangement of cations. Positive values of Q thus indicate a degree of normal ordering in spinels, while the negative values indicate some inverse ordering. Of the systems studied, $MgAl_2O_4$, $ZnAl_2O_4$ and $FeAl_2O_4$ are classified as normal spinels and $NiAl_2O_4$ and $MgFe_2O_4$ as inverse.

For each spinel, we have calculated (Lavrentiev et al., 2003a, 2004) the order parameter, Q, over a broad temperature range, as shown in Fig. 1. This figure also compares our calculated values of Q at zero pressure with experimental data (Redfern et al., 1999; Harrison et al., 1998; Waerenborgh et al., 1994; O'Neill et al., 1991, 1992). The calculated value of Q for the normal spinels gradually decreases on heating. Above approximately

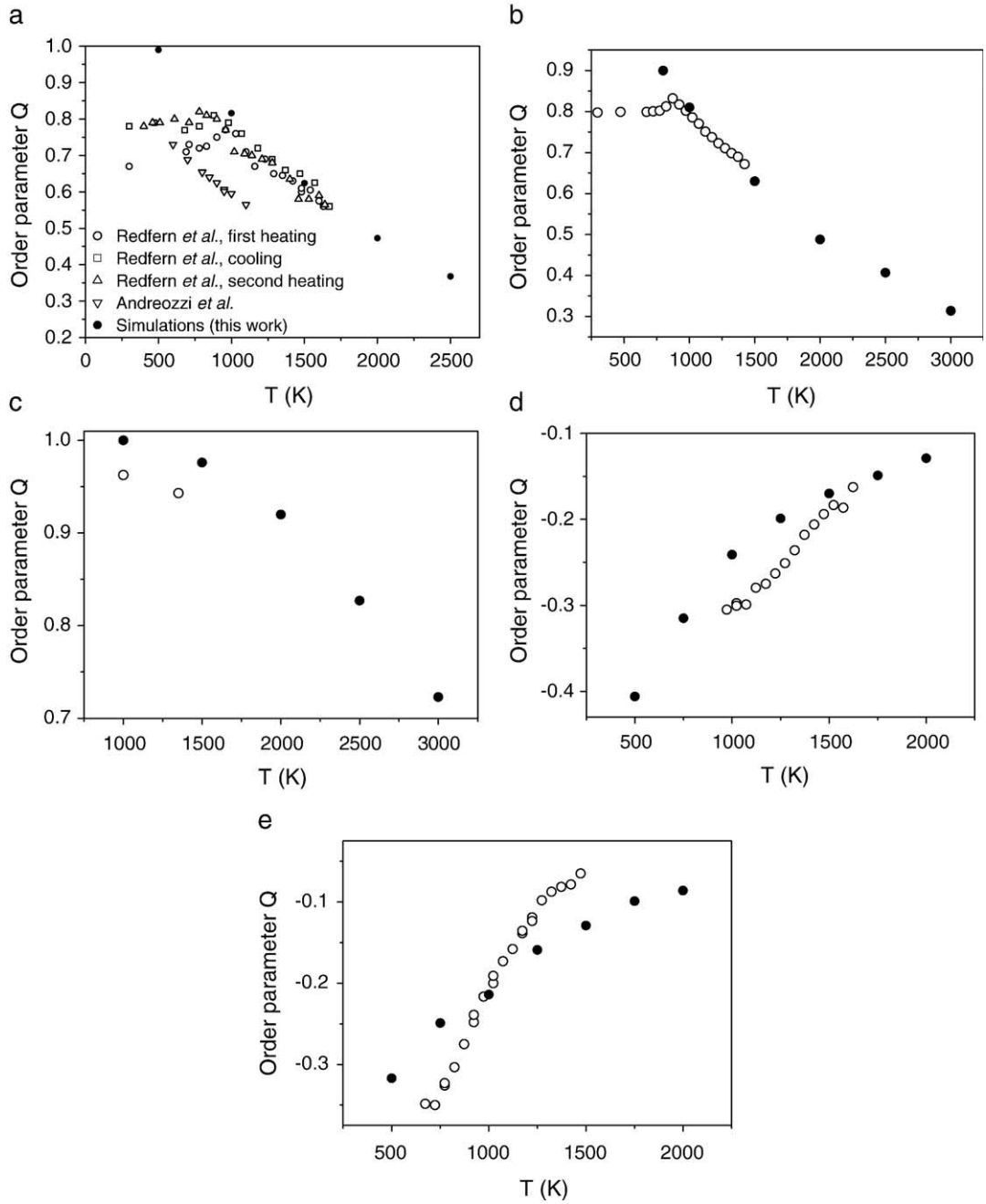

Fig. 1. Calculated values (solid circles) of the order parameter, Q, vs. T for (a) $MgAl_2O_4$, (b) $FeAl_2O_4$, (c) $ZnAl_2O_4$, (d) $NiAl_2O_4$ and (e) $MgFe_2O_4$. The data are compared with the experimental results of (a) Redfern et al. (1999) and Andreozzi et al. (2000), (b) Harrison et al. (1998), (c) Waerenborgh et al. (1994), (d) O'Neill et al. (1991) and (e) O'Neill et al. (1992). Experimental data shown as open circles in (b–e). Symbols for experimental data for $MgAl_2O_4$ are explained directly in (a).

900–1000 K, our results show excellent agreement with the experiments of Redfern et al. (1999). Below this temperature kinetic effects, which are not included in our calculations, become increasingly important. Our results for $MgAl_2O_4$ display similar features to those calculated using a parameterised Hamiltonian (Warren et al., 2000). This is not unexpected due to the similar nature of the computational technique, even though that of Warren et al. (2000) does not include thermal effects. The variation of Q with temperature, if not the absolute value of Q itself, is similar in the two studies. Of the three normal spinels studied, $ZnAl_2O_4$ shows the wea-

kest temperature dependence of the order parameter (Q changes from 1 to 0.72 between 1000 K and 3000 K). In contrast to the normal spinels, the calculated value of Q for the inverse spinels increases with temperature. Our calculated values are not in as good agreement with experiment as for the normal spinels, but are nevertheless still able to provide qualitative and quantitative information. The derivative $\partial Q/\partial T$ is similar for both compounds, according to our simulations, while experiment suggests a higher value for $MgFe_2O_4$. It is worth noting in this context that earlier experiments (Tellier, 1967; Faller and Birchenall, 1970) gave lower values of $\partial Q/\partial T$, in better agreement with our simulations. Finally, it is worth noting that increasing the temperature to 2000 K leads to an almost random arrangement of cations ($Q \approx -0.1$) in inverse spinels, while for all normal spinels studied, a large degree of order remains even at this temperature ($0.5 \leq Q \leq 0.9$).

The Monte Carlo technique allows us to investigate the dependence of the bulk modulus and thermal expansion coefficient on the order parameter. Recently, Hazen and Yang (1999) (see also Smyth et al., 2000) have derived equation-of-state parameters, such as compressibility and thermal expansion, for spinels from bond distances, bond compressibilities, and bond thermal expansivities, which, in turn, are estimated from crystal chemical systematics. They propose the degree of cation order–disorder strongly affects both the bulk modulus and the thermal expansion, and in particular their calculations suggest that the compressibilities for normal (fully ordered) and completely inverse variants may differ by as much as 17% ($MgTi_2O_4$), with linear thermal expansivities differing by 15% ($MgAl_2O_4$, $MgFe_2O_4$). We have therefore performed calculations for (completely) normal and (completely) inverse spinels at 1000 K and zero pressure. During the simulation, the value of the order parameter Q was kept constant (i.e., 1 for normal and -0.5 for inverse spinel), so that the normal spinel is completely ordered and exchanges between cations are prohibited, while in the inverse spinel, exchanges between A- and B-type cations on octahedral sites are still possible. The results are collected together in Table 1. Our results indicate that the bulk modulus and the linear expansion coefficient exhibit a marked dependence on Q. The biggest difference between normal and inverse spinels is for the calculated thermal expansion coefficient, which is as large as 21% for $NiAl_2O_4$ and $MgFe_2O_4$. For the bulk modulus, the largest difference is for $NiAl_2O_4$ (9%). Our conclusions for the expansion coefficient agree with those of Hazen and Yang (1999) in that normal $MgAl_2O_4$ and $MgFe_2O_4$ have larger expansion coefficients than the inverse structures. However, Hazen and Yang (1999) also suggest the bulk modulus is larger for the normal structures, whereas our simulations suggest the contrary. This discrepancy is possibly due to the values of bond compressibility used by Hazen and Yang (1999), which were taken from high-pressure structure studies and cannot be directly applied at zero pressure. In addition, their results for the inverse structure depend on the procedure chosen to average bond distances and the derivatives of these quantities with respect to pressure.

Table 1
Calculated bulk moduli and thermal expansion coefficients for normal and inverse spinels at 1000 K

System	Type of ordering	Bulk modulus (GPa)	Linear expansion coefficient (10^{-6} K^{-1})
Spinel ($MgAl_2O_4$)	Normal	170	8.8
	Inverse	180	8.1
Hercynite ($FeAl_2O_4$)	Normal	166	9.8
	Inverse	181	8.4
Gahnite ($ZnAl_2O_4$)	Normal	158	10.3
	Inverse	161	9.3
$NiAl_2O_4$	Normal	165	10.0
	Inverse	180	8.3
Magnesioferrite ($MgFe_2O_4$)	Normal	144	11.6
	Inverse	155	9.6

For the normal spinels, we predict the order parameter is almost independent of pressure (Fig. 2). Increasing the pressure leads to a slight decrease of the order parameter for $MgAl_2O_4$ and hercynite $FeAl_2O_4$, and to a very small increase in Q for gahnite $ZnAl_2O_4$. The results for $MgAl_2O_4$ appear to be consistent with the known resistance of this material to void swelling under neutron radiation, which, it has been suggested, is linked to only a small volume change accompanying interchange of the Mg and Al ions (Sickafus et al., 2000). The pressure effect is more pronounced for inverse spinels, and especially for $NiAl_2O_4$. For both inverse spinels, the degree of inversion for a given temperature increases with increasing pressure.

3.2. MgO–MnO surface

All the surface MC calculations were undertaken on 20 MnO–MgO layers in region I and 40 layers in region II. The surface was expanded to generate unit cell containing 72 surface cations. The lattice parameters for the MgO/MnO unit cell were held fixed at those obtained in a previous bulk MC simulation in the *NPT* ensemble at the appropriate temperature. In order to simplify the calculations, we have neglected segrega-

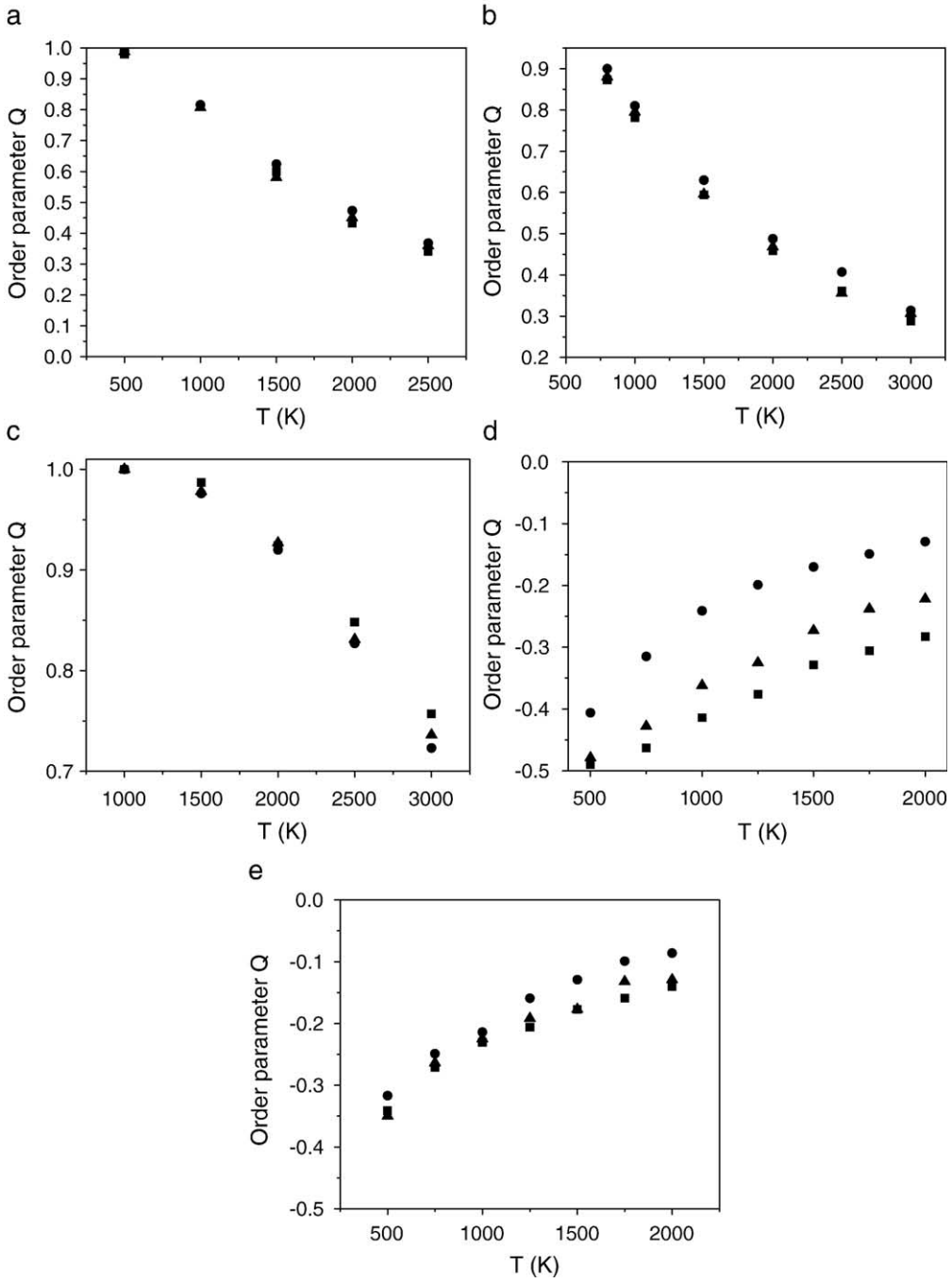

Fig. 2. Calculated temperature variation of the order parameter at zero and high pressure for (a) $MgAl_2O_4$, (b) $FeAl_2O_4$, (c) $ZnAl_2O_4$, (d) $NiAl_2O_4$ and (e) $MgFe_2O_4$. Results are given for $P=0$ (solid circles), $P=10$ GPa (solid triangles) and $P=20$ GPa (solid squares).

tion to kinks, steps or dislocations which real crystals undoubtedly possess. The particular set of empirical short-range interaction potentials employed is that of Lewis and Catlow (1985), first introduced in their study of the parent oxides, and used here with a cut-off of 10 Å.

Fig. 3 displays the fractional surface coverage of Mn^{2+} ions at the {001} surface as a function of the overall mole fraction χ of Mn^{2+} present in the bulk solid solution over a range of temperatures. The straight line in Fig. 3 shows the behaviour expected if there were no segregation to or from the surface. The surface

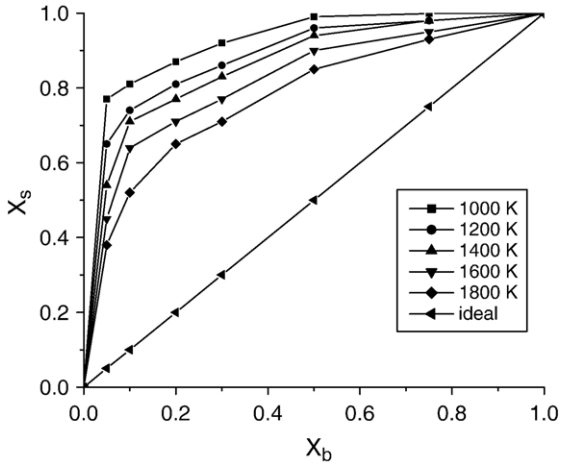

Fig. 3. Fractional surface coverage of Mn^{2+} ions, X_s, plotted as a function of the bulk Mn^{2+} concentration, X_b, at different temperatures for the {001} surface.

concentration of Mn^{2+} increases sharply as a function of overall concentration, with enrichment of the surface layer by the larger Mn^{2+} ion at *all* temperatures for *all* compositions.

At other than the highest Mn^{2+} concentrations, the surface concentration of Mn^{2+} ions varies strongly with temperature, as also clearly shown in Fig. 3, with a marked decrease in the surface enrichment by Mn^{2+} with increasing temperature. For example, for an overall 20% Mn^{2+} composition ($\chi = 0.2$), the fractional surface coverage decreases from ≈ 0.87 to ≈ 0.65 as the temperature increases from 1000 K to 1800 K. In addition, the ratio Mn^{2+}/Mg^{2+} decreases rapidly as a function of depth (Fig. 4). We do not see any oscillatory subsurface behaviour as noted by Battaile et al. (1995) in their mean-field simulation studies of similar systems.

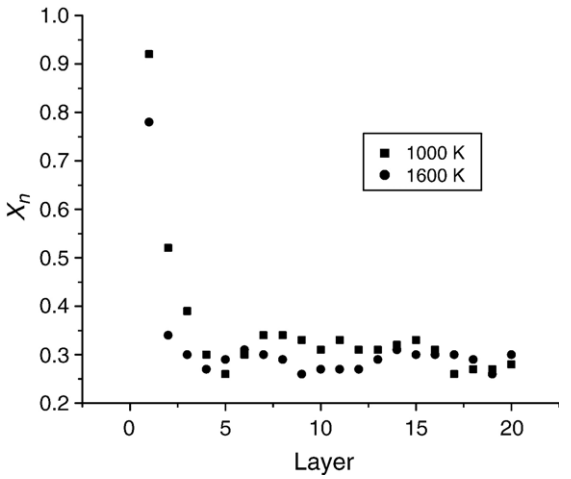

Fig. 4. The atomic ratio of Mn^{2+} ions, X_n, as a function of depth for an overall concentration, X_b, of 0.3.

3.3. Phase diagram of MnO/MgO at high pressures

Monte Carlo simulations at a given temperature in the semi-grand canonical ensemble yield the calculated variation of $\Delta\mu_{Mg/Mn}$ with composition. As in the Margules approximation (e.g., Thompson, 1967), we write the excess (non-ideal) free energy as a third degree polynomial in the concentration:

$$G_{excess} = (W_1 x_2 + W_2 x_1) x_1 x_2 \tag{17}$$

where x_1 and x_2 are the mole fractions of the components and the W are asymmetric interaction parameters: W_1, for example, is the energy of putting component 1 into component 2, and vice versa. The chemical potential difference then consists of an ideal solution term and a second degree polynomial:

$$\frac{\Delta\mu}{k_B T} = \frac{\Delta\mu_0}{k_B T} + \ln\left(\frac{x_1}{x_2}\right) + W_1 x_2 (1 - 3x_1) - W_2 x_1 (1 - 3x_2). \tag{18}$$

The results for $\Delta\mu$ at each temperature were fitted to a curve of the form of Eq. (18). Integration then gives the variation of free energy with composition, and the resulting ΔG_{mix} vs. composition curves are shown in Fig. 5.

The calculation of the free energy of mixing employing QLD is a severe test of the procedure since ΔH_{mix} and $-T\Delta S_{mix}$ are often very close in magnitude and attention has to be paid to the convergence of the results

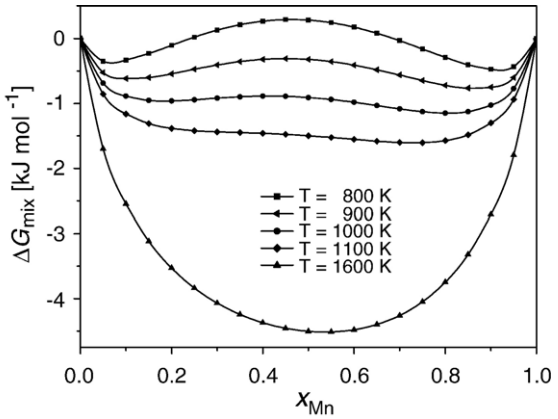

Fig. 5. Variation of ΔG_{mix} (kJ mol^{-1}) for MnO–MgO with composition. These results have been calculated for a range of temperatures using exchange Monte Carlo (MCX).

with respect to both cell size and the number of configurations sampled (Todorov et al., 2004). Nevertheless, for MnO–MgO 250 configurations with a supercell of 128 atoms are sufficient to ensure adequate convergence in the positions of the two minima in the ΔG_{mix} vs. composition curves in Fig. 6, which plots ΔG_{mix} vs. x_{Mn} for this cell size over a wide range of temperatures. These curves are similar to those obtained in Fig. 5 using MC. The *vital* importance of allowing for atomic relaxation is shown strikingly in Fig. 7 which compares calculated ΔG_{mix} vs. composition curves at 1000 K with and without relaxation. In the absence of relaxation, ΔG_{mix} is *positive* for all compositions studied, which illustrates, dramatically, the importance of relaxation. There is also good agreement between ΔS_{mix} values obtained via the Monte Carlo free energy and enthalpy of mixing and those obtained from QLD (Todorov et al., 2004).

Common tangent constructions to the data in Fig. 5 yield the calculated phase diagrams and spinodals in Fig. 8. Also shown in the figure are those obtained by de Villiers et al. (1998) using the experimental data of Wood et al. (1994). The agreement between the QLD and MCX simulations is good, and our results provide strong support for the experimental results of Wood et al. (1994), ruling out the formation of a complete solid solution at temperatures as low as 600 K. The calculated phase diagram possesses a marked asymmetry with MnO less soluble in MgO than MgO in MnO. The same type of asymmetry is also observed in the CaO/MgO system, with the smaller cation more soluble in CaO than the larger cation in MgO. The phase diagram obtained from the measurements of Wood et al. (1994) is more asymmetric than those calculated.

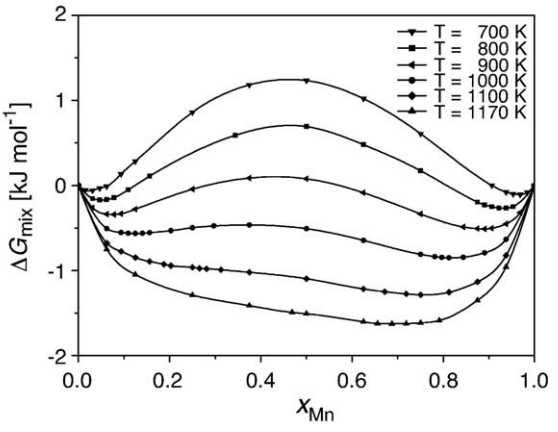

Fig. 6. Variation of ΔG_{mix} (kJ mol^{-1}) for MnO–MgO with composition. These results have been calculated for a range of temperatures using configurational lattice dynamics (QLD).

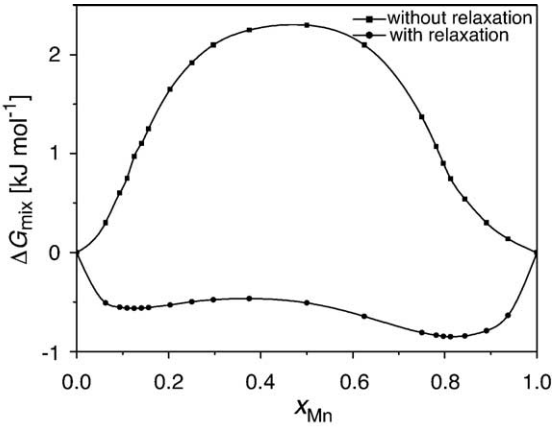

Fig. 7. Variation of ΔG_{mix} (kJ mol^{-1}) for MnO–MgO with composition for $T=1000$ K. The results have been calculated with and without atomic relaxation and demonstrate the importance of relaxation.

de Villiers et al. (1998) have discussed the experimental errors and conclude this asymmetry should be smaller.

It is straightforward to repeat the calculations for thermodynamic properties at any pressure. To illustrate this, we turn to consider the behaviour of the MnO–MgO system at 50 GPa. No phase transitions are expected at this pressure. Neither MnO or MgO undergo a phase transition until the pressure is well in excess of this figure. Fig. 9 also shows the calculated phase diagram for MnO/MgO at 50 GPa obtained using QLD and MCX. We see that there is excellent agreement between QLD and MCX at both 0 GPa and 50 GPa.

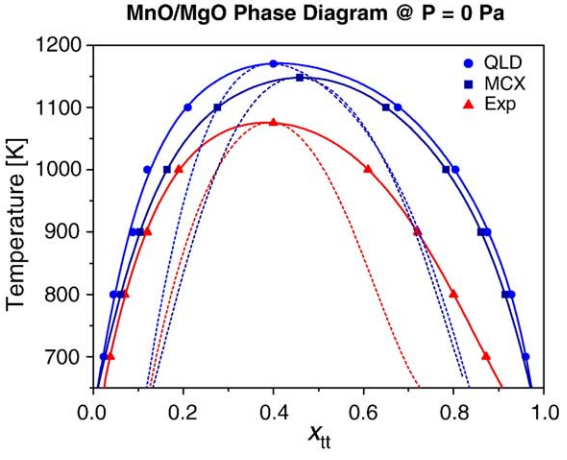

Fig. 8. Phase diagram for MnO–MgO calculated at zero pressure using QLD (circles) and MCX (squares). The calculated data are compared with the experimental results (triangles) of de Villiers et al. (1998).

3.4. Configurational lattice dynamics—(Ca,Mg)CO_3 mixing

Carbonates contribute a significant portion of the Earth's crust but have proved experimentally challenging, e.g., Land (1998), and there is still considerable debate concerning dolomite formation. Thus, order/disorder in dolomite and the nature of calcite-rich phases are an ideal candidate for simulation (e.g., Fisler et al., 2000; Burton and van de Walle, 2003) and we have attempted to model dolomite, the most abundant carbonate, using configurational averaging techniques. Dolomite, $Ca_xMg_{(1-x)}(CO_3)_2$, has a hexagonal structure with planes of cations (Ca or Mg) separated by planes of carbonates.

Our calculations used a 72-cation unit cell (total atom number 360) over a range of compositions. In order to reduce computer time, minimisations were performed in the static limit (i.e., vibrational effects have been neglected) and approximately 25,000 configurations were sampled for each composition. In Fig. 10, we present the calculated phase diagram of dolomite. The agreement with experiment is encouraging, with reproduction of all the main features. The main differences lie close to the end members and are largely a consequence an artefact of the small cell size used, which limits the concentration range in these composition regions.

We have found, in agreement with previous studies (Fisler et al., 2000; Wright et al., 2002; Burton and van de Walle, 2003), that the ordering is very dependent on the positions of the cations, particularly the cations adopting homogeneous cation layers. This results from the large difference in cation radii between Ca^{2+} (1.00 Å) and Mg^{2+} (0.72 Å) so that any positioning of a Mg or Ca ion within a layer dominated by the other will disrupt the ideal cation positions. Fisler et al. (2000) have analysed the enthalpy difference between the ordered and disordered 50:50 dolomite phases and estimated the enthalpy difference of disorder to be 34.4 kJ mol^{-1}. Calorimetric experiments have predicted a value of 35.8 kJ mol^{-1} (Navrotsky et al., 1999). Comparing a fully disordered lattice, where no ordered layers are formed, with the ordered dolomite we find an energy difference of 24.6 kJ mol^{-1}. The size of the energy gap between ordered and disordered phases is significant at all mixes and we see that higher energy disordered states are only accessible at temperatures beyond approximately 600 K.

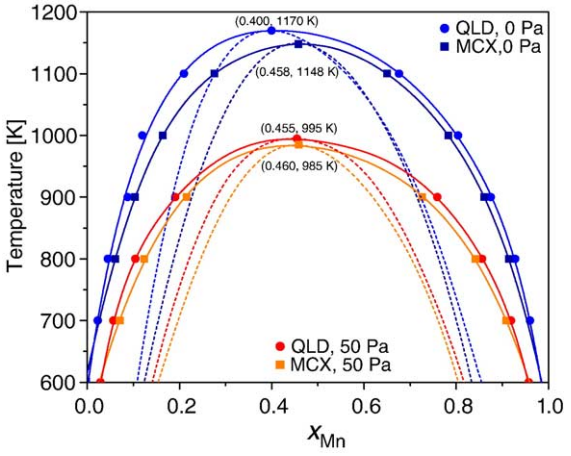

Fig. 9. A comparison of calculated phase diagrams at (QLD and MCX) of MgO–MnO at 0 and 50 GPa. Consolute temperatures and corresponding compositions are marked in each case.

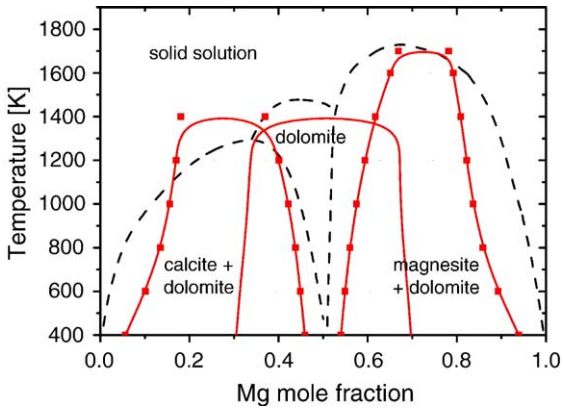

Fig. 10. Phase diagram of the dolomite system. The solid lines are calculated points and the dashed lines are the experimental results of Goldsmith et al. (1962).

4. Final remarks

Solid solutions of ionic compounds have traditionally proved problematic for the theoretician. We have presented a range of methods for the simulation of such solid solutions and their surfaces, the accurate calculation of thermodynamic quantities of mixing, and also for the calculation of phase diagrams. All the methods sample many configurations, explicitly considering different arrangements of ions, and allow for the *local* structural relaxation surrounding each cation. This relaxation is crucial. If ignored, the energy of exchange of any two ions is usually very high and all exchanges are rejected, thus sampling only one arrangement. The role of vibrational effects is unclear. For example, in Ni_3Al the experimental difference in vibrational entropy between the ordered and disordered phases is approximately $0.2k_B$ (Fultz et al., 1995). The origin of this difference is controversial and may be due to a nearly

uniform softening of modes caused by the increased volume of the disordered phase (Ravelo et al., 1998) or a significant decrease in the number of high frequency vibrational modes during the disordering process (Anthony et al., 1993). Purton et al. (1998) have demonstrated that excluding atomic vibrations from the simulation influences the degree of ordering in $MgMnSiO_4$; see also the detailed discussion of Todorov et al. (2004).

The techniques are applicable over ranges of pressure and/or temperature. Disorder problems are often tackled by using a general Ising model, simplified by limiting interactions to a short range and a finite number of multisite couplings. Such an approach can be awkward to parameterise for ionic solids, where relaxation is crucial, and to apply over a range of pressures and temperatures. It is not readily generalised to less symmetric structures, to which we also wish to apply the general methodology outlined here. In our methodology, no assumptions are made as to the nature of the solid solution.

The Monte Carlo and the configurational averaging methods each have their own strengths and advantages. Monte Carlo techniques are applicable to the solid at high temperatures and to melts (Purton et al., 2000; Lavrentiev et al., 2003b). The semi-grand canonical ensemble is an attractive route to differences in chemical potential and consequent calculation of the free energy and the phase diagram. QLD is efficient and gives the free energies to high precision. Moreover, quantum effects are included in the vibrational contributions at low temperatures. Further work is in progress to develop and extend all the methods, e.g., Monte Carlo simulation of order/disorder involving vacancy disorder, hybrid Monte Carlo/molecular dynamics methods and Monte Carlo simulations employing the transmutational ensemble in order to study the partitioning and segregation of trace elements at grain boundaries (Hiraga et al., 2004).

Acknowledgements

This research was funded by EPSRC grant GR/M53899 and computational facilities were provided by two HEFCE JREI awards. We would like to thank Prof. S.C. Parker and an anonymous reviewer for commenting on the manuscript. **[LW]**

References

Allan, N.L., Barrera, G.D., Fracchia, R.M., Lavrentiev, M.Yu., Taylor, M.B., Todorov, I.T., Purton, J.A., 2001a. Free energy of solid solutions and phase diagrams via quasiharmonic lattice dynamics. Phys. Rev., B 63 (art. no. 094203).

Allan, N.L., Blundy, J.D., Purton, J.A., Lavrentiev, M.Y., Wood, B.J., 2001b. Trace element incorporation in minerals and melts, in Solid Solutions in Silicate and Oxide Systems, ed. Geiger, C.A., volume 3 of the European Mineralogical Union Notes in Mineralogy, series editors Papp, G., and Weiszburg, T.G. Budapest: Eötvös University Press, Ch. 11, 251–302.

Allen, M.P., Tildesley, D.J., 1987. Computer Simulation of Liquids. Oxford University Press.

Andreozzi, G.B., Princivalle, F., Skogby, H., Della Giusta, A., 2000. Cation ordering and structural variations with temperature in $MgAl_2O_4$ spinel: an X-ray single-crystal study. Am. Mineral. 85, 1164–1171.

Anthony, L., Okamoto, J.K., Fultz, B., 1993. Vibrational entropy of ordered and disordered Ni_3Al. Phys. Rev. Lett. 70, 1128–1130.

Barrera, G.D., Taylor, M.B., Allan, N.L., Barron, T.H.K., Kantorovich, L.N., Mackrodt, W.C., 1997. Ionic solids at elevated temperatures and high pressures: MgF_2. J. Chem. Phys. 107, 4337–4344.

Battaile, C.C., Najafabadi, R., Srlovitz, D.J., 1995. Simulation of segregation to free surfaces in cubic oxides. J. Am. Ceram. Soc. 78, 3195–3200.

Burton, B.P., van de Walle, A., 2003. First principles-based calculations of the $CaCO_3$–$MgCO_3$ and $CdCO_3$–$MgCO_3$ subsolidus phase diagrams. Phys. Chem. Miner. 30, 88–97.

Carpenter, M., Salje, E.K.H., 1994. Thermodynamics of nonconvergent cation ordering in minerals: II. Spinels and the orthopyroxene solid solution. Am. Mineral. 79, 1068–1083.

Catlow, C.R.A., 1997. Computer Modelling in Inorganic Crystallography. Academic, London.

Catlow, C.R.A., Mackrodt, W.C., 1982. Theory of simulation methods for lattice and defect energy calculations in crystals. In: Catlow, C.R.A., Mackrodt, W.C. (Eds.), Computer Simulation of Solids. Springer-Verlag, Berlin, pp. 3–20. Chapter 1.

Chadi, D.J., Cohen, M.L., 1973. Special points in the Brillouin zone. Phys. Rev., B 8, 5747–5753.

de Villiers, J.P.R., Buseck, P.R., Steyn, H.S., 1998. MnO exsolution in periclase from Langban, Sweden: an evaluation of the activity–composition relations in the system MgO–MnO. Min. Mag. 62, 333–339.

Dick, B.G., Overhauser, A.W., 1958. Theory of the dielectric constants of alkali halide crystals. Phys. Rev. 112, 90–103.

Faller, J.G., Birchenall, C.E., 1970. The temperature dependence of ordering in magnesium ferrite. J. Appl. Crystallogr. 3, 496–503.

Fisler, D.K., Gale, J.D., Cygan, R.T., 2000. A shell model for the simulation of rhombohedral carbonate minerals and their point defects. Am. Mineral. 85, 217–224.

Frenkel, D., Smit, B., 2002. Understanding Molecular Simulation. 2nd ed. Academic Press, San Diego.

Fultz, B., Anthony, L., Nagel, L.J., Nicklow, R.M., Spencer, S., 1995. Phonon densities of states and vibrational entropies of ordered and disordered Ni_3Al. Phys. Rev., B 52, 3315–3321.

Goldsmith, J.R., Graf, D.L., Witters, J., Northrop, D.A., 1962. Studies in the system $CaCO_3$–$MgCO_3$–$FeCO_3$: 1. Phase relations: 2. A method for major-element spectrochemical analysis: 3. Compositions of some ferroan dolomites. J. Geol. 70, 659–688.

Harrison, R.J., Putnis, A., 1999. The magnetic properties and crystal chemistry of oxide spinel solid solutions. Surv. Geophys. 19, 461–520.

Harrison, R.J., Redfern, S.A.T., O'Neill, H.St.C., 1998. The temperature dependence of the cation distribution in synthetic hercynite

($FeAl_2O_4$) from in-situ neutron structure refinements. Am. Mineral. 83, 1092–1099.
Hazen, R.M., Downs, R.T. (Eds.), 2000. High-Temperature and High-Pressure Crystal Chemistry, Volume 41 of Reviews in Mineralogy and Geochemistry. The Mineralogical Society of America, Washington.
Hazen, R.M., Yang, H., 1999. Effects of cation substitution and order–disorder on *P–V–T* equations of state of cubic spinels. Am. Mineral. 84, 1956–1960.
Hiraga, T., Anderson, I.M., Kohlstedt, D.L., 2004. Grain boundaries as reservoirs of incompatible elements in the Earth's mantle. Nature 427, 699–703.
Land, L.S., 1998. Failure to precipitate dolomite at 25 °C from dilute solution despite 1000-fold oversaturation after 32 years. Aquat. Geochem. 4, 361–368.
Lavrentiev, M.Yu., Allan, N.L., Barrera, G.D., Purton, J.A., 2001. Ab initio calculation of phase diagrams of oxides. J. Phys. Chem., B 105, 3594–3599.
Lavrentiev, M.Yu., Purton, J.A., Allan, N.L., 2003a. Ordering in spinels—a Monte Carlo study. Am. Mineral. 88, 1522–1531.
Lavrentiev, M.Yu., Allan, N.L., Purton, J.A., 2003b. Beyond the point defect limit: solid solutions, phase diagrams and trace element partitioning. Phys. Chem. Chem. Phys. 5, 2190–2196.
Lavrentiev, M.Yu., Purton, J.A., Allan, N.L., 2004. Ordering in spinels—a Monte Carlo study. Reply. Am. Mineral. 89, 1149.
Lewis, G.V., Catlow, C.R.A., 1985. Potential models for ionic oxides. J. Phys. C 8, 1149–1161.
Mackrodt, W.C., Stewart, R.F., 1977. Defect properties of ionic solids: point defects at the surfaces of face-centred cubic crystals. J. Phys. C 10, 1431–1445.
Maradudin, A.A., Montroll, E.W., Weiss, G.H., Ipatova, I.P., 1971. Theory of Lattice Dynamics in the Harmonic Approximation/Solid State Phys., Suppl. 3, 2nd ed. Academic Press, New York (NY).
Metropolis, N., Rosenbluth, A.W., Rosenbluth, M.N., Teller, A.N., Teller, E., 1953. Equation of state calculations by fast computing machines. J. Chem. Phys. 21, 1087–1092.
Navrotsky, A., 1994. Physics and Chemistry of Earth Minerals (Cambridge Topics in Mineral Physics and Chemistry, 6). Cambridge University Press.
Navrotsky, A., Kleppa, O.J., 1967. The thermodynamics of cation distributions in simple spinels. J. Inorg. Nucl. Chem. 29, 2701–2714.
Navrotsky, A., Dooley, D., Reeder, R., Bradly, P., 1999. Calorimetric studies of the energetics of order–disorder in the system $Mg_{1-x}Fe_xCa(CO_3)_2$. Am. Mineral. 84, 1622–1626.
O'Neill, H.S.C., Dollase, W.A., Ross II, C.R., 1991. Temperature dependence of the cation distribution in nickel aluminate ($NiAl_2O_4$) spinel: a powder XRD study. Phys. Chem. Miner. 18, 302–319.
O'Neill, H.St.C., Annersten, H., Virgo, D., 1992. The temperature dependence of the cation distribution in magnesioferrite ($MgFe_2O_4$) from powder XRD structural refinements and Mössbauer spectroscopy. Am. Mineral. 77, 725–740.
Purton, J.A., Barrera, G.D., Allan, N.L., Blundy, J.D., 1998. Monte Carlo and hybrid Monte Carlo/molecular dynamics approaches to order–disorder in alloys, oxides and silicates. J. Phys. Chem., B 102, 5202–5207.
Purton, J.A., Allan, N.L., Blundy, J.D., 1999. Phase transitions in disordered solids via hybrid Monte Carlo: the orthorhombic to cubic phase transition in $(Mg,Mn)SiO_3$ perovskite. Chem. Commun. 8, 707–708.
Purton, J.A., Blundy, J.D., Allan, N.L., 2000. Computer simulation of high-temperature, forsterite–melt partitioning. Am. Mineral. 85, 1087–1091.
Ravelo, R., Aguilar, J., Baskes, M., Angelo, J.E., Fultz, B., Holian, B.L., 1998. Free energy and vibrational entropy differences between ordered and disordered Ni_3Al. Phys. Rev., B 57, 862–869.
Redfern, S.A.T., Harrison, R.J., O'Neill, H.St.C., Wood, D.R.R., 1999. Thermodynamics and kinetics of cation ordering in $MgAl_2O_4$ spinel up to 1600 °C from in situ neutron diffraction. Am. Mineral. 84, 299–310.
Rittner, J.D., Foiles, S.M., Seidman, D.N., 1994. Simulation of surface segregation free energies. Phys. Rev., B 50, 12004–12014.
Sickafus, K.E., Minervini, L., Grimes, R.W., Valdez, J.A., Ishimaru, M., Li, F., McClellan, K.J., Hartmann, T., 2000. Radiation tolerance of complex oxides. Science 289, 748–751.
Smyth, J.R., Jacobsen, S.D., Hazen, R.M., 2000. Comparative crystal chemistry of dense oxide minerals. In: Hazen, R.M., Downs, R.T. (Eds.), High-Temperature and High-Pressure Crystal Chemistry, Reviews in Mineralogy and Geochemistry vol. 41. Mineralogical Society of America, pp. 157–186.
Tasker, P.W., 1979. The surface energies, surface tensions and surface structure of the alkali halide crystals. Philos. Mag., A 39, 119–130.
Taylor, M.B., Barrera, G.D., Allan, N.L., Barron, T.H.K., 1997. Free-energy derivatives and structure optimization within the quasiharmonic approximation. Phys. Rev., B 56, 14380–14390.
Taylor, M.B., Barrera, G.D., Allan, N.L., Barron, T.H.K., Mackrodt, W.C., 1998. SHELL: a code for lattice dynamics and structure optimisation of ionic crystals. Comput. Phys. Commun. 109, 135–143.
Tellier, J.-C., 1967. Sur la substitution dans le ferrite de magnésium des ions trivalents, tétravalents et pentavalents. Rev. Chim. Miner. 4, 325–365.
Thompson, J.B., 1967. In: Abelson, P.H. (Ed.), Researches in Geochemistry vol. II. John Wiley, New York, p. 340.
Todorov, I.T., Allan, N.L., Lavrentiev, M.Y., Freeman, C.L., Mohn, C.E., Purton, J.A., 2004. Simulation of mineral solid solutions at zero and high pressure using lattice statics, lattice dynamics and Monte Carlo methods. J. Phys., Condens. Matter 16, S2651–S2770.
Waerenborgh, J.C., Figueiredo, M.O., Cabral, J.M.P., Pereira, L.C.J., 1994. J. Solid State Chem. 111, 300–309.
Wallace, D.C., 1972. Thermodynamics of Crystals. Wiley, New York (NY). 484 pp.
Warren, M.C., Dove, M.T., Redfern, S.A.T., 2000. Ab initio simulations of cation ordering in oxides: application to spinel. J. Phys., Condens. Matter 12, L43–L48.
Wood, B.J., Hackler, R.T., Dobson, D.P., 1994. Experimental determination of Mn–Mg mixing properties in garnet, olivine and oxide. Contrib. Mineral Petrol. 115, 438–448.
Wright, K., Cygan, R.T., Slater, B., 2002. Impurities and nonstoichiometry in the bulk and on the (1014) surface of dolomite. Geochim. Cosmochim. Acta 66, 2541–2546.